Journal of Power Sources 246 (2014) 55–62

Contents lists available at ScienceDirect

Journal of Power Sources

journal homepage: www.elsevier.com/locate/jpowsour

The use of poly(vinyl phosphonic acid) microgels for the preparation of inherently magnetic Co metal catalyst particles in hydrogen production

Nurettin Sahiner [a,b,*], Selin Sagbas [a]

[a] Faculty of Science & Arts, Chemistry Department, Canakkale Onsekiz Mart University, Terzioglu Campus, 17100 Canakkale, Turkey
[b] Nanoscience and Technology Research and Application Center (NANORAC), Canakkale Onsekiz Mart University, Terzioglu Campus, 17100 Canakkale, Turkey

GRAPHICAL ABSTRACT

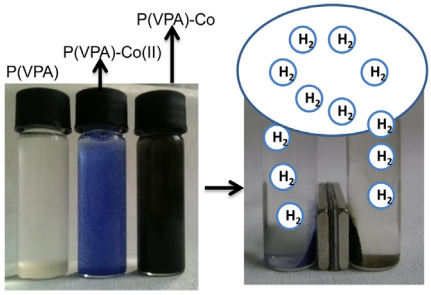

ARTICLE INFO

Article history:
Received 2 May 2013
Received in revised form
3 July 2013
Accepted 8 July 2013
Available online 26 July 2013

Keywords:
Hydrogel-composite
Porous poly(vinyl phosphonic acid)
microgel reactors
Nanogel composites
Hydrogen production

ABSTRACT

Novel poly(vinyl phosphonic acid) (p(VPA)) micro particle and composite p(VPA)–silica micro particle hydrogels are synthesized using a micro-emulsion polymerization technique. Porous p(VPA) particles are generated after removal of silica particles upon treatment of composite p(VPA) with 0.5 M NaOH solution. Bare, composite with silica, and porous p(VPA) micro particle hydrogels are used as templates and as reactors. Metal nanoparticles, Co, Ni, and Cu are generated in situ inside these hydrogels by chemical reduction of the absorbed metal ions with a reducing agent such as sodium boron hydride ($NaBH_4$), and are used as catalyst in hydrogen production by hydrolysis of $NaBH_4$ in a basic medium and ammonia borane (AB). The effects of reloaded metal ions, the reaction temperature, the porosity, the reusability, and the type of metal (Co, Ni, Cu) are investigated. The activation energy for hydrolysis of $NaBH_4$, and AB by p(VPA)–Co is 28.02 and 25.51 kJ mol^{-1}, respectively. The mass susceptibility measurements of composite p(VPA)–Co microgel is found as ferromagnetic. It is found that p(VPA) microgels provided better catalytic performance in comparison to macro p(VPA) hydrogels due to improved properties such as higher surface area, pore structure, and inherently magnetic behavior after multiple loadings-reduction of Co(II) from aqueous medium.

1. Introduction

Microgels are generally described as hydrogels with cross-linked polymeric particles below 100 nm that can be swollen by a good solvent. The high water content of microgels makes them soft and elastic with increased and tunable physical characteristics and

* Corresponding author. Faculty of Science & Arts, Chemistry Department, Canakkale Onsekiz Mart University, Terzioglu Campus, 17100 Canakkale, Turkey. Tel.: +90 2862180018 2041; fax: +90 2862181948.
E-mail address: sahiner71@gmail.com (N. Sahiner).

0378-7753/$ – see front matter © 2013 Elsevier B.V. All rights reserved.
http://dx.doi.org/10.1016/j.jpowsour.2013.07.043

these properties provide great resemblance to soft tissues [1,2]. These natural characteristics of microgels, with tunability of size, shape and functional groups in addition to their easy fabrication and processing techniques, makes them indispensable materials in drug delivery [3–5], actuation, biosensing [6,7], catalysis [8,9] and chemical separation [9].

Recently, porous materials have attracted great attention and undergone rapid development due to their adjustable pore structure and multifunctionality that can be achieved by tailoring the composition, structure, chemical composition and surface properties [10]. They are also in great demand as scientific and technological materials because of their high surface area and ability to adsorb/absorb and interact with different species such as atoms, molecules, and ions. Various inorganic and organic materials are employed as starting materials to combine with a hydrogel precursor as templates for the design and fabrication of porous microgels. Using silica precursors during microgel particle preparation allows composite material synthesis with adaptable surface and pore structure as silica particles are dissolvable via NaOH or HF treatments [11]. Therefore, materials generated in this way, in combination with the natural characteristics of microgels, can merge their inherent properties to generate novel devices [12,13].

Recently, hydrogen was assumed to replace fossil fuels as a greener and renewable energy carrier alternative due to their attractive properties such as environmental friendliness, high energy density, non-toxic reaction products. Hydrogen with an energy density of 142 MJ kg^{-1} has a higher energy carrier potential compared with petroleum (42 MJ kg^{-1}) [14]. Efficient, safe and convenient hydrogen storage and supply systems are the most important issues to circumvent to allow the use of hydrogen in industrial applications. Hydrogen is one of the important factors to meet Department of Energy (DOE) targets for fuel cell commercialization. Although almost half of the cost reduction is achieved for the target of DOE put forward that is $30/kW by 2015, the cost is still over 50% higher than the target of DOE [15]. Polymer electrolyte membrane (PEM) fuel cell can use hydrogen as source of energy and can directly convert chemical energy stored in fuels such as hydrogen to electrical energy. Therefore, fundamental studies have great significance for hydrogen powered system with higher output and better yield including water and heat management, and the development of new materials for providing safe and pure hydrogen for improved fuel cell performance with feasible cost [15].

Hydrogen also can be stored in the form of atomic hydrogen in metal hydrides or chemical hydrides [16]. Chemical hydrides, such as $NaBH_4$, NH_3BH_3 (ammonia borane), $NaAlH_4$, CaH_2, MgH_2, and $LiBH_4$, are the most commonly used materials for hydrogen storage. Amongst them, $NaBH_4$ and ammonia borane (AB) are the most convenient materials as storage and supply systems due to their advantages, such as high gravimetric/volumetric hydrogen storage capacity (10.8 wt %) for $NaBH_4$, and (19.6 wt %) for AB compared to other metal hydrides. Additionally, their nontoxic nature, non-flammability in basic aqueous solution, high stability in air, and the ability to control the hydrogen production can provide additional advantages. Moreover, the reaction byproducts, $NaBO_2$ can be recycled, and H_2 generation even at low temperatures can be possible with an exothermic hydrolysis reactions. Ideal $NaBH_4$ and AB hydrolysis reaction occurs according to the following reactions [16–20].

$$NaBH_4 + 2H_2O \xrightarrow{\text{catalyst}} NaBO_2 + 4H_2 \quad (1)$$

$$Na_3BH_3 + 2H_2O \xrightarrow{\text{catalyst}} NH_4^+ + BO_2^- + 3H_2 \quad (2)$$

There has been an increased interest in using microgels as microreactors for templated synthesis of inorganic and/or metal nanoparticles [21]. Transition metal nanoparticles cannot be used directly as catalyst due to aggregation and destabilization [22]. Hydrogel, microgel and nanogel materials were employed as template for in situ metal nanoparticle preparation using nickel, copper, cobalt, silver, and ruthenium and then used as catalyst for various reactions [23–26]. Moreover, these hydrogel–metal composites can be used in numerous other applications such as sensors, optics, electronics, actuators, and microfluidic devices as well as separation devices for different purposes [21]. Earlier we reported the use of p(AMPS) microgels for the in situ preparation of Co and Ni metal nanoparticles as templating material and the catalyst for hydrolysis reactions of $NaBH_4$ or AB [13].

Here, we report vinyl phosphonic acid (VPA) microgel use for the same purpose. As VPA has widespread applications, such as in the design and modification of surfaces due to strong metal complexation ability, heat and hydrolysis stability, and even as a medium for adhesion and proliferation of cells due to their hydrophilic (phosphonic acid) and lipophilic (vinyl) functional groups. Therefore, we aim to synthesize novel poly(vinyl phosphonic acid) (p(VPA)) micro particle and composites as p(VPA)–silica micro particle hydrogels via a photo polymerization technique. Porosity was generated in p(VPA) microgels after removal of silica moieties upon treatment of composite p(VPA)–silica with 0.5 M NaOH solution. Then the microgel particles were used as a template for loading Co, Ni, and Cu ions into the microgel network and then reduced to generate the corresponding metal nanoparticles (Co, Ni, Cu) and they were used in hydrolysis reactions of $NaBH_4$ or AB to generate hydrogen. Various parameters that affect the hydrolysis of $NaBH_4$ and/or AB such as metal species, the amount of metal catalyst, the sequential metal loading-reduction cycles, the porosity, the reaction temperature, and the reusability were investigated. Moreover, we also report magnetic behavior of Co(II) ions and Co nanoparticles within p(VPA) microgels as inherently magnetic particles can also be used in hydrolysis of $NaBH_4$ and/or AB. This is very important as there is no need for magnetic ferrite inclusion within p(VPA) microgel to control hydrogen generation with an externally applied magnetic field [18].

2. Experimental

2.1. Materials

Vinyl phosphonic acid (VPA, 90%) as monomer, *N*,*N*′-methylenebisacrylamide (MBA) as crosslinkers, and 2,2′-azobis(2-methylpionamidine) dihydrochloride as photo-initiator, lecithin, as a surfactant in granular form were purchased from Aldrich, and Acros chemical companies, and gasoline (95 octane) as a solvent procured from a local gas station. Tetraethyl orthosilicate (TEOS, 99%, Merck), sodium hydroxide (NaOH, 98%, Aldrich) were used as received. $NaBH_4$ (Merck, 98%) as reduction agent and cobalt (II) chloride hexahydrate ($CoCl_2 \cdot 6H_2O$, 99% Sigma–Aldrich) and nickel (II) chloride hexahydrate ($NiCl_2 \cdot 6H_2O$, 97%, Riedel-de Haën) were used as metal ion sources. Distilled water (Millipore Direct-Q3 UV) was used throughout the experiments.

2.2. Synthesis of the p(VPA) particles

P(VPA) particles in micrometer dimensions were synthesized using a micro-emulsion polymerization technique. In short, the crosslinker (MBA, 0.75% mol ratio with respect to VPA) was dissolved in 5 ml VPA monomer, and 80 mg UV initiator solution (2,2′-azobis(2-methylpionamidine) dihydrochloride) was prepared by dissolving in 200 μl DI water. This UV initiator solution was added to VPA solution, and then 0.5 ml of this mixture was dispersed in 15 ml 0.1 M lecithin solution in gasoline. Then the reaction was irradiated in a photo reactor (LUZCHEM, 420 nm, Canada) for 4 h for simultaneous

polymerization of crosslinking under vigorous stirring at 1200 rpm. The obtained VPA micro particles were purified by centrifugation at 24 683 *g* for 10 min at 20 °C. Firstly, the supernatant solution was removed and washed with cyclohexane to remove lecithin. Then the particles were washed with ethanol–water mixture two times to remove the unreacted (monomer, surfactant, crosslinker, and initiator) particles. The obtained particles were dried at 40 °C and kept in a closed container for further use.

2.3. Synthesis of p(VPA)–silica composite and porous p(VPA) particles

A composite material, p(VPA)–silica micro particles, were prepared according to the method reported in the literature with some modifications [13]. Briefly, to 0.5 ml of the mixture prepared as above, containing monomer, crosslinker, and UV-initiator, was added 0.25 ml of TEOS and mixed to thoroughly disperse in 15 ml 0.1 M lecithin solution in gasoline. Then, the same steps were carried out as described in Section 2.2. To form porous p(VPA) particles, p(VPA)–silica composite particles were treated with 0.5 M NaOH solution for 24 h under 500 rpm mixing rate to dissolve silica particles. Then the excess NaOH was neutralized with 0.1 M HCl until pH of the solution reached 7. The resultant porous p(VPA) micro particles were washed by centrifugation in acetone at least two times, dried at 40 °C and used for further studies.

2.4. Porosity measurements

The specific surface areas of the particles were evaluated using the Brunauer–Emmett–Teller (BET) method. The pore volume, and average pore sizes were also evaluated using the Barret–Joyner–Halenda (BJH) method. BET measurement was obtained using a Tristar II Surface Area and Porosity Analyzer. P(VPA) microgels were degassed to remove moisture and other contaminants at 120 °C for 6 h prior to adsorption analysis. This was done using a Flow Prep 060 Degasser.

2.5. In situ preparation of Co, Ni, and Cu nanoparticles within p(VPA)-based micro particle

Different metal ions such as Co, Ni, and Cu were loaded into the microgel, and their corresponding metal nanoparticles were prepared inside the microgel similar to previously reported studies [21]. For this purpose, 100 mg p(VPA) microgels were placed in 50 ml of 500 ppm metal ion solutions (Co(II), Ni(II) or Cu(II)) for 2 h to load the metal ions into the microgels. Then, the metal ion-loaded microgels were washed with DI water to remove unbound metal ions from the microgel network. To form metal nanoparticles within p(VPA) microgels, these metal ion-loaded hydrogels were transferred to 100 ml of 0.2 M aqueous $NaBH_4$ solution for 2 h until completion of reduction of the bound metal ions. As an indication of the particle formation no more gas evolution was observed and these metal nanoparticle-containing p(VPA) composites were washed with DI water several times and were dried at 40 °C, and used as catalyst systems in the hydrolysis of $NaBH_4$ and AB.

2.6. Characterization of p(VPA) and composite p(VPA)–metal based particles

The IR spectra of p(VPA)-based micro particles were recorded using a Perkin–Elmer FT-IR spectroscope. The absorbance measurements were carried out within the spectral range of 650–4000 cm^{-1} using attenuated total reflectance (ATR) with 4 cm^{-1} resolution.

The thermal characterization and the metal content of p(VPA) microgels measurements were carried out using a thermo gravimetric analyzer (SII TG/DTA 6300). Approximately 5 mg of p(VPA)-based particles were placed in TGA pans and the weight lost against temperature in the range of 50–1000 °C was recorded at a heating rate of 10 °C min^{-1} under a dry flow of N_2 of 100 ml min^{-1}.

The amounts of metal nanoparticles within p(VPA) composite microgels were determined with AAS (Thermo, ICA 3500 AA SPECTRO) measurements for the solution obtained by three treatments of p(VPA)–M composites with 50 ml 5 M HCl solution to dissolve the metal nanoparticles from the microgel composites.

Magnetic mass susceptibility (χ_g) measurements of 0.1 g bare p(VPA), Co(II) ion-absorbed p(VPA), and Co^0 nanoparticle-loaded p(VPA)–Co composite were carried out using a magnetic susceptibility balance (MSB mk1) at room temperature. Magnetic mass susceptibility was calculated as $\chi_g^{cgs} = [(\text{length of tube filled in cm}/\text{mass of sample in tube in g})^*C^*(R - Ro)]$. Where, *R* and *Ro* are the mass of the empty tube and the sample mass in the tube, respectively. *C* is a constant 1^*10^{-9}.

2.7. Hydrolysis of $NaBH_4$ and AB catalyzed by p(VPA)–metal microgel composites

In the hydrolysis reactions of $NaBH_4$ and AB, certain amounts of p(VPA)–metal microgel composite containing equal amounts of Co, Ni, and Cu nanoparticles were placed into 50 ml water (containing 5 wt % NaOH for $NaBH_4$ hydrolysis) at 30 °C. To initiate the hydrolysis reaction, 50 mM (0.0965 g) $NaBH_4$ or (0.077 g) AB were added to this reaction mixture and stirred at 1000 rpm. The volume of produced hydrogen gas with time was measured via an inverted volumetric cylinder. All the experiments were repeated three times, and the results were presented as the mean values with standard deviations.

To determine the effect of metal nanoparticle species in hydrolysis of $NaBH_4$ and AB, certain amounts of p(VPA)–M microgel composites containing the same amount of Co and Ni (0.232 mmol) were used as catalyst systems under the same reaction conditions. The hydrolysis conditions for $NaBH_4$ were 50 mM 50 ml aqueous $NaBH_4$ solution containing 5 wt % NaOH, at 30 °C, 1000 rpm mixing rate and for AB, 50 mM 50 ml aqueous AB solution at 30 °C, 1000 rpm mixing rate without NaOH.

To determine the effect of sequential loading-reduction cycles of Co(II) on the hydrolysis of $NaBH_4$, 0.1 g p(VPA) was used as catalyst system under the same reaction conditions (50 mM 50 ml aqueous $NaBH_4$ solution containing 5 wt % NaOH, at 30 °C, 1000 rpm mixing rate).

For kinetic studies, five times metal ion-loaded 0.1 g p(VPA) microgels were tested for $NaBH_4$ and AB hydrolysis at 30, 50, and 70 °C under the same reaction conditions.

In order to study the effect of porosity on the hydrolysis of $NaBH_4$, known amounts of p(VPA)–Co, and porous p(VPA)–Co composite microgels containing 0.232 mmol Co were used as catalyst systems, and compared in terms of their catalytic performances at the same reaction conditions (50 mM 50 ml aqueous $NaBH_4$ solution containing 5 wt % NaOH, at 30 °C, 1000 rpm).

In order to study the reusability of catalyst systems, 0.1 g microgel–Co composite was used 10 times consecutively in one day under the same reaction conditions (50 mM 50 ml aqueous $NaBH_4$ solution containing 5 wt % NaOH at 30 °C).

3. Results and discussion

3.1. Synthesis, characterization and the determination of the amount of metal particles within p(VPA)-based microgel

Bulk p(VPA) hydrogel with macro dimensions were shown for use as template in the preparation of metal nanoparticles such as

Co, Ni, and Cu [27,28]. Here, we synthesized p(VPA), composite p(VPA)–Si, and porous p(VPA) micro particles using water-in-oil micro emulsion technique and used them as template for Co, Ni, and Cu nanoparticle preparation within the microgel network, and then as catalysts for H_2 production in hydrolysis of $NaBH_4$ and AB. The preparation of p(VPA) in a smaller dimension can offer better catalytic performances for their in situ prepared metal nanoparticles and tunable porosities by inclusion of silica moieties. The p(VPA)-based particles were synthesized with MBA crosslinker as demonstrated in Fig. 1a. Optical microscope images of p(VPA), Ni(II) ion and Co(II) ion-absorbed, and Co or Ni nanoparticle-containing p(VPA) microgels are shown in Fig. 1b. It is obvious that p(VPA) microgels are spherical in shape. The particle sizes vary from a few hundred nm to 20 μm. To generate additional pores in p(VPA) microgels, the prepared p(VPA)–Si composite was treated with 0.5 M NaOH to remove the silica particles.

The FT-IR spectra of VPA monomer, p(VPA) particles, p(VPA)–Si composite, and por-p(VPA) microgels were recorded and are shown in Fig. 2. The specific bands for VPA monomer were identified as the wide band at about 3500 cm^{-1} corresponding to OH stretching, and wide bands between 2900 and 2550 cm^{-1} and the peaks at 1615 and 1110 cm^{-1} belonging to P=O stretching coming from phosphonic acid. p(VPA) and por-p(VPA) microgels crosslinked with

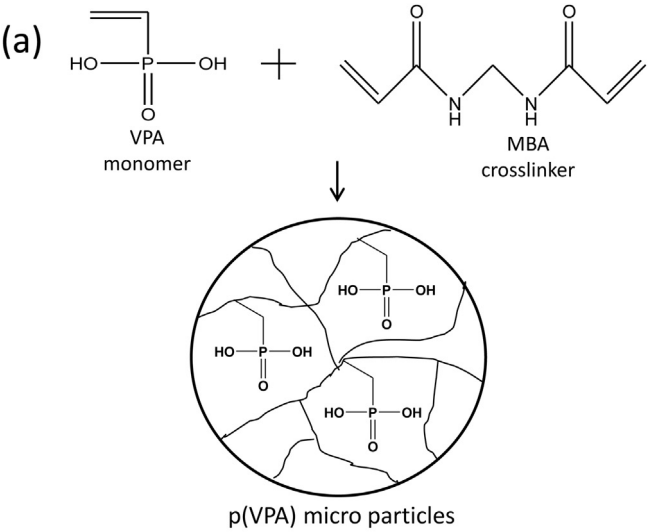

Fig. 1. (a) Representation of crosslinking p(VPA) microgel with MBA. (b) Optical microscope images of bare (1), Ni(II) (2) and Co(II) (3) absorbed, and Co or Ni nanoparticle-containing (4) of p(VPA) microgels.

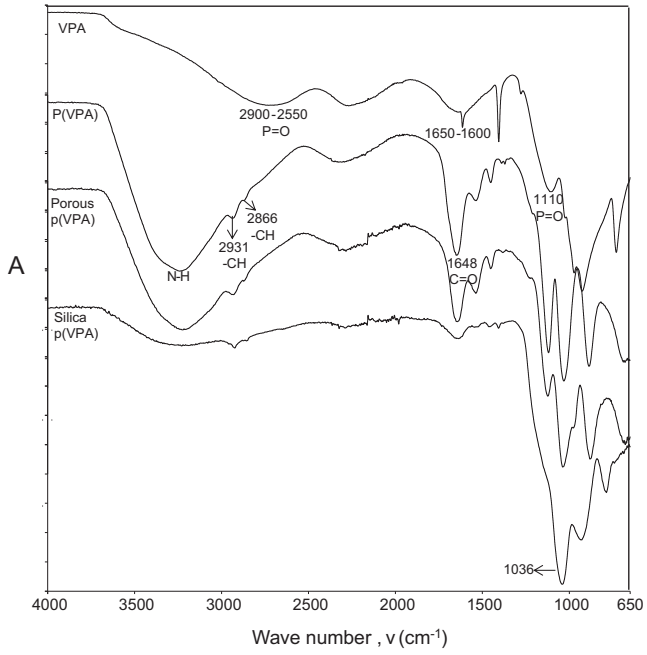

Fig. 2. FT-IR analysis of VPA, p(VPA), por-p(VPA), and p(VPA)–Si microgels.

MBA also showed these typical bands, a broad band at 3600 with 3200 cm^{-1} corresponding to N–H stretching, the peaks at 2931 and 2866 cm^{-1} belonging to –C–H stretching, and the peak at about 1648 cm^{-1} for C=O stretching belonging to the crosslinker MBA. The composite p(VPA)–Si microgels also have the same specific bands as p(VPA) microgels but additionally the characteristic bands of silica also appear at about 1036 cm^{-1}, corresponding to Si–O stretching. As can be seen from the FTIR spectra of p(VPA)-based microgels, p(VPA) particles successfully formed with MBA crosslinker, and silica particles were removed by 0.5 M NaOH treatment of the composite p(VPA)–Si microgel creating porous p(VPA) microgels. To determine the amount of metal nanoparticles inside composite p(VPA)–M microgels, thermogravimetric analysis was performed on p(VPA), p(VPA)–Cu, p(VPA)–Ni and p(VPA)–Co microgels as illustrated in Fig. 3a. As can be seen from the thermograms of the p(VPA) microgels, the degradations start about 110 °C and 440 °C for all the samples. The initial degradation could be due to water loss from the hydrophilic networks. The TG analysis revealed that the metal content of p(VPA)–Cu, p(VPA)–Ni and p(VPA)–Co microgels are about 41.9, 43.6, and 47.2 wt % for Cu, Ni, and Co. Moreover, TGA was also used to determine the Co nanoparticle content of the multiple Co(II) loaded and reduced p(VPA) microgels. Loading and reduction processes were sequentially repeated five times. TGA results show that the metal content of the 1st loading of p(VPA)–Co microgels was about 47.2 wt %, however, the metal content of 5th loading of p(VPA)–Co microgels was about 62.79 wt % as given in Table 1. In order to determine the exact amount of metal in composite p(VPA)–M microgels, the metal nanoparticles were dissolved by 50 ml 5 M HCl, and the metal ion amounts were determined by AAS measurements. As can be seen from Table 1, the amounts of Co(II) ion increased with the metal loading and reduction cycle number. p(VPA)–Co composite was loaded with 136.67 mg g^{-1} Co ions for initial Co loading-reduction, and after two, three, four, and five Co loading-reduction cycles, p(VPA)–Co microgels absorbed 308.94, 389.36, 544.42, and 760.28 mg g^{-1} Co ions, respectively. Table 2 shows p(VPA)–M composite microgels metal loading capacity for different metal ions for example, p(VPA) microgel absorbs 136.67 mg g^{-1} Co ions,

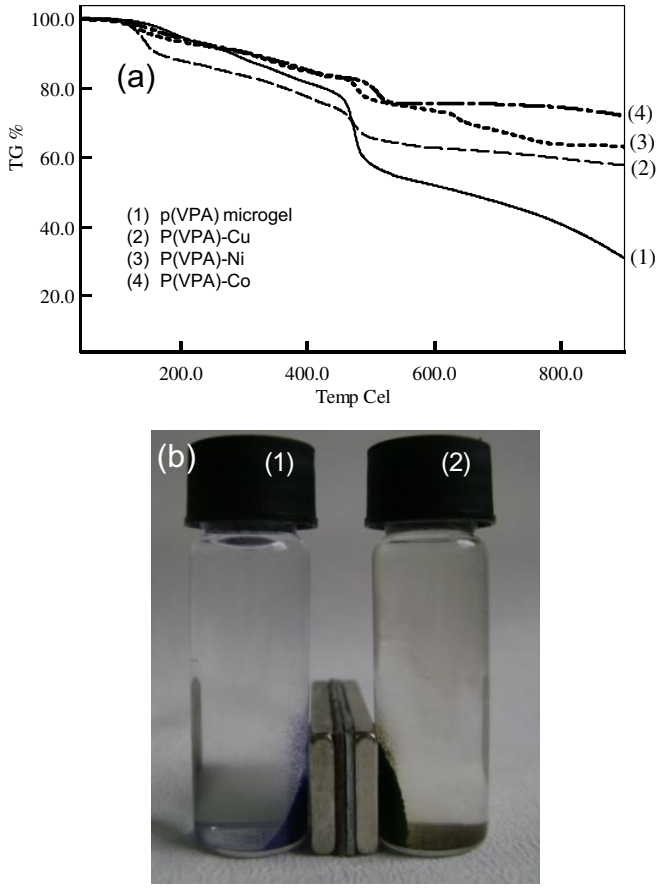

Fig. 3. (a) TGA thermograms of p(VPA) and composite p(VPA)–M microgel [containing M: 41.9 wt % of Cu, 43.6 wt of % Ni, 47.2 wt % of Co composites]. (b) Digital camera images of (1) Co(II) and (2) Co nanoparticle loaded p(VPA) particles behavior under an externally applied magnetic field.

Table 1
The amount of cobalt nanoparticles inside p(VPA)–Co microgel composite catalysts prepared by sequential loading.

P(VPA) microgel–Co	AAS (mg g^{-1})	TG (Residue %)
1. Loading	136.6 ± 6.2	47.2 ± 1.1
2. Loading	308.9 ± 11.3	53.2 ± 3.6
3. Loading	389.3 ± 4.1	55 ± 2.4
4. Loading	544.4 ± 20.2	57.4 ± 3.1
5. Loading	760.2 ± 35.4	62.7 ± 4.5

112.6 mg g^{-1} Ni ions, and 104.84 mg g^{-1} Cu ions, whereas, porous p(VPA)–M microgels absorbed 176.7 mg g^{-1} Co determined by AAS measurements. Therefore, porous p(VPA) microgels have more metal loading capacity than p(VPA) microgel due to the better accessibility of functional groups within the microgel network after the removal of silica.

Table 2
The amount of metal nanoparticles inside p(VPA)–M and porous p(VPA)–Co microgel composite catalysts.

Microgel–M composite	[a]AAS (mg g^{-1})		
	Co	Ni	Cu
p(VPA)	136.6 ± 6.2	112.6 ± 2.3	104.8 ± 7.4
Porous p(VPA)	176.7 ± 9.9		

[a] All metal ion amounts were measured per 1 g p(VPA) microgel.

Table 3
Magnetic susceptibility of p(VPA) and p(VPA)–Co based microgels.

Microgel–M composites	Mass susceptibility (χ_g^{cgs})	Susceptibility mechanism
p(VPA)	$-1.1 \times 10^{+10}$ cm^3 g^{-1}	Diamagnetism
Co^{+2} absorbed p(VPA)	4.1×10^{-6} cm^3 g^{-1}	Paramagnetism
Co^0 loaded p(VPA)–Co composite	1	Ferromagnetism

As can be seen in the digital camera images in Fig. 3b, the aqueous solution of dispersed Co(II)-absorbed (1), and Co nanoparticle-containing (2) p(VPA) particles change colors from violet to black respectively, and their behavior under externally applied magnetic field as shown in (1) and (2). The Co(II)-absorbed p(VPA) particles have a weak magnetization, whereas, the Co-loaded p(VPA) particles have a strong magnetization by an externally applied magnetic field. Magnetic susceptibility (χ) of a material is the degree of magnetization in response to an applied magnetic field. The metal ions and metal nanoparticles within the microgel network exhibited different magnetic behaviors. The magnetic mass susceptibilities (χ_g^{cgs}) of bare p(VPA) and Co ion-absorbed p(VPA) were measured in MSB and calculated as $-1.1 \times 10^{+10}$ and 4.1×10^{-6} cm^3 g^{-1}, respectively, as illustrated in Table 3. Bare p(VPA), and Co(II) ions absorbed p(VPA) particles showed diamagnetic and paramagnetic behavior, however, Co nanoparticles possess quite a different behavior. The results confirm that the prepared composite p(VPA)–Co microgels here are naturally ferromagnetic and may have great potential as naturally magnetic catalyst materials. Earlier, we report the use magnetic ferrite particle together with metal nanocatalyst such as Ru in the controllable hydrogen production from hydrolysis of $NaBH_4$ [18]. Here we report the inherently magnetic Co nanoparticles as both catalyst and magnetic particles. These provide additional advantages such as the direct use of catalyst instead of magnetic ferrites for controlling the hydrogen generation by an externally applied magnetic field.

3.2. The effect of metal species on the hydrogen production from the hydrolysis of $NaBH_4$ and NH_3BH_3

To determine the effect of the metal species on hydrogen production from the hydrolysis of $NaBH_4$ and AB, the same amount of metal nanoparticles (0.232 mmol)-containing p(VPA) microgel, as composite p(VPA)–M (M: Co, Ni, Cu), were used. For example, 0.1 g p(VPA)–Co and 0.121 g p(VPA)–Ni microgel composites were used in hydrolysis of 50 mM 50 ml aqueous $NaBH_4$ solution containing 5 wt % NaOH at 30 °C and 1000 rpm mixing rate. As demonstrated in Fig. 4a, 250 ml H_2 gas was produced with p(VPA)–Co microgels in 13 min, whereas the same amount of H_2 gas was produced with p(VPA)–Ni microgels in 31 min. So, p(VPA)–Co composite has better activity than p(VPA)–Ni microgel catalyst system. Again, 0.1 g p(VPA)–Co, 0.121 g p(VPA)–Ni, and 0.141 g p(VPA)–Cu microgels containing the same amount of metal nanoparticles (0.232 mmol) were used in the hydrolysis of 50 ml 50 mM AB at 30 °C and 1000 rpm mixing rate as illustrated in Fig. 4b, they all produced 178 ml H_2. The times to produce this amount were different e.g., p(VPA)–Co microgels produce it in 4 min, whereas p(VPA)–Ni and p(VPA)–Cu microgels produce this amount in 8.5 min and 27 min, respectively. As can be seen from Table 4, the total turnover frequencies (TOF) for the $NaBH_4$ hydrolysis reaction were calculated as 3.31 mol H_2 (mol catalyst min)$^{-1}$ for p(VPA)–Co, and 1.39 mol H_2 (mol catalyst min)$^{-1}$ for p(VPA)–Ni. The hydrogen generation rate (HGR) for Co, Ni, and Cu-loaded microgels for the AB hydrolysis reaction were 3272, 1538, and 447 (ml H_2) (g of metal

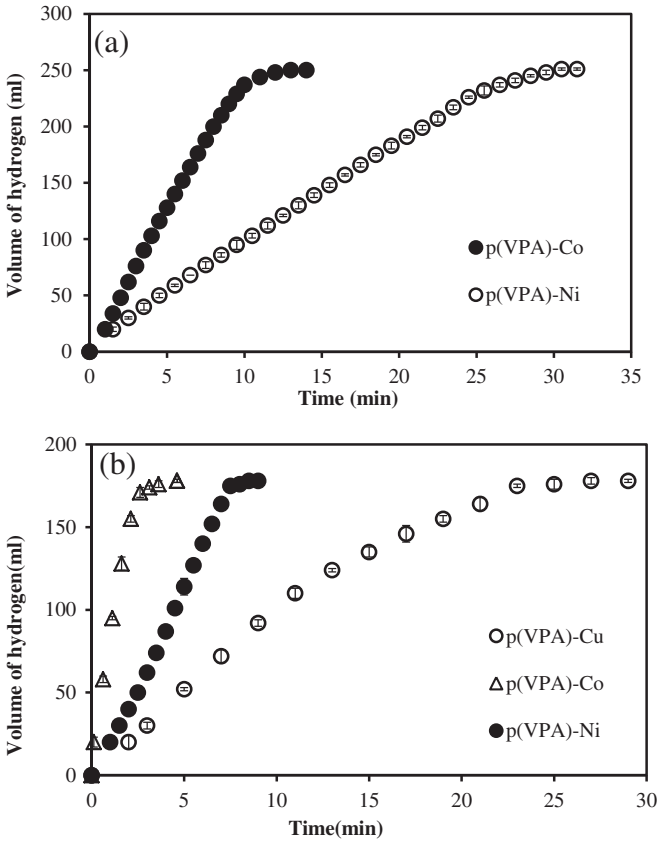

Fig. 4. (a) The effect of metal species on $NaBH_4$ hydrolysis by p(VPA)–M microgels composite [M: Co and Ni each 0.232 mmol, 50 mM 50 ml aqueous $NaBH_4$ solution containing 5 wt % NaOH, at 30 °C, 1000 rpm]. (b) The effect of metal species on ammonia borane hydrolysis by p(VPA)–M microgels composite [M: Co, Ni, and Cu each 0.232 mmol, 50 mM 50 ml aqueous AB solution at 30 °C, 1000 rpm].

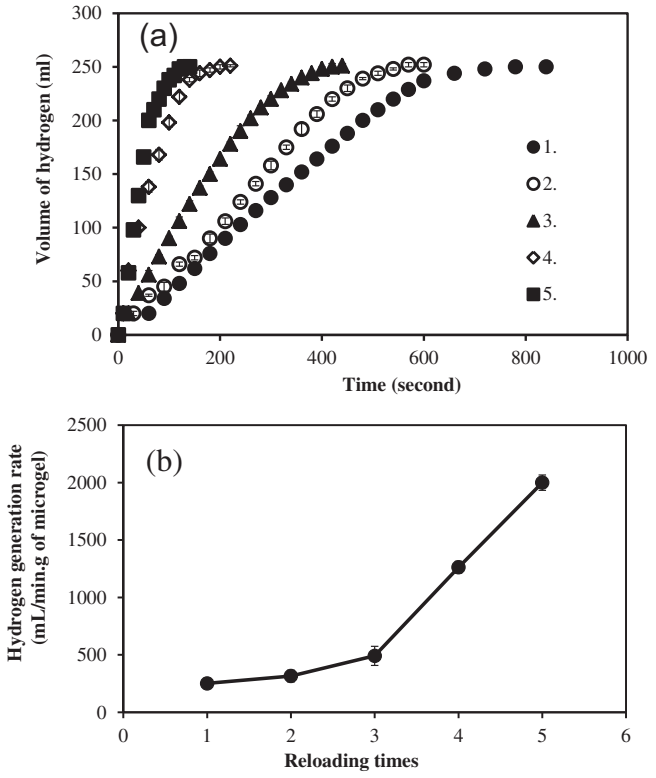

Fig. 5. The effect of (a) sequential loading and (b) their hydrogen generation rates (HGR) on the hydrolysis of $NaBH_4$ by 0.1 g p(VPA)–Co microgel composite [50 mM 50 ml aqueous $NaBH_4$ solution containing 5 wt % NaOH, at 30 °C, 1000 rpm].

min)$^{-1}$, respectively. The total TOF for the AB hydrolysis reaction were calculated as 7.67 mol H_2 (mol metal min)$^{-1}$ for p(VPA)–Co, 3.61 mol H_2 (mol metal min)$^{-1}$ for p(VPA)–Ni, and 1.13 mol H_2 (mol metal min)$^{-1}$ for p(VPA)–Cu. The HGR for the $NaBH_4$ hydrolysis reaction were calculated as 1407 (ml H_2) (g of Co min)$^{-1}$ for p(VPA)–Co, and 592 (ml H_2) (g of Ni min)$^{-1}$ for p(VPA)–Ni. The HGR values of 1127 (ml H_2) (min g)$^{-1}$ for carbon supported Co–B catalysts [29], and 400 (ml H_2) (min.g)$^{-1}$ for Ni–Ru nanocomposite catalysts were reported [30]. P(VPA)–Co composite microgels, among the other catalysts, seem to be the most efficient catalyst for hydrogen generation systems. For the metal nanoparticles loaded in the same p(VPA) microgel matrixes, hydrogen produced rates is in the order of Co > Ni > Cu nanoparticles. In the literature, many metals and alloys catalysts have been used for $NaBH_4$ and AB hydrolysis reactions. Demirci and Garin studied catalytic performance of different RuM (M: Cu, Pd, Ag, Pt) and PtAg alloys [31] and reported that Ru and RuPt alloys have the same catalytic performance but alloying with inactive metals such as Cu, Pd, Ag increased the performance of Ru. In the our previous studies, The HGR and total TOF for $NaBH_4$ hydrolysis reaction by bulk p(AMPS)–Ru were 7462 (ml H_2) (g of metal min)$^{-1}$ and 30.35 mol H_2 (mol metal min)$^{-1}$ [18]. From the literature, Ru nanoparticles provide very fast catalytic performance in different hydrolysis reactions [18] however; the metal catalysts, Co, Ni, and Cu, reported here are cheap and readily prepared as they are conveniently available.

Table 4
The comparison of HGR and TOF in the hydrolysis of $NaBH_4$ and AB by various catalyst systems.

Catalyst	*T* (°C)	Metal content (mmol)	Hydrogen generation rates (ml H_2) (g of Co min)$^{-1}$		Total turn over frequency (mol H_2) (mol catalyst min)$^{-1}$	
			$NaBH_4$	AB	$NaBH_4$	AB
p(VPA)–Ni micro	30	0.232	592	1538	1.39	3.61
p(VPA)–Cu micro	30	0.232	–	447	–	1.13
p(VPA)–Co micro	30	0.232	1407	3272	3.31	7.67
p(VPA)–Co micro 2. loading	30	0.524	852	–	2	–
p(VPA)–Co micro 3. loading	30	0.66	879	–	2.07	–
p(VPA)–Co micro 4. loading	30	0.92	1282	–	3	–
p(VPA)–Co micro 5. loading	30	1.29	1572	1603	3.69	3.78
p(VPA)–Co micro 5. loading	50	1.29	2631	2725	6.57	6.79
p(VPA)–Co micro 5. loading	70	1.29	5681	5855	15.02	15.59
Por-p(VPA)–Co micro	30	0.232	2033	–	4.78	–
p(VPA)–Co bulk	30	0.122	2345	–	5.46	–
p(Aam-co-VPA)–Co bulk	30	0.15	1142	–	2.66	–
P(AMPS)–Ru bulk	30	0.03	7462		30.35	

3.3. The effect of metal reloading on the hydrogen production rate

The effect of sequential loading-reduction of Co ions on the hydrolysis of $NaBH_4$ was determined by using 0.1 g p(VPA)–Co microgel containing 0.232 mmol Co for 50 mM 50 ml aqueous $NaBH_4$ solution containing 5 wt % NaOH at 30 °C. As shown in Fig. 5a, the first time metal-loaded microgel produced 250 ml H_2 in 780 s, whereas when sequentially second, third, fourth, and fifth time metal-loaded microgels produced 250 ml H_2 in 570, 440, 220, and 130 s, respectively. The total TOF values of 1st, 2nd, 3rd, 4th, and 5th time metal loadings were 3.31, 2.008, 2.075, 3.006, and 3.691 mol H_2 (mol metal min)$^{-1}$, respectively. The HGR of 1st, 2nd, 3rd, 4th, and 5th time metal loading were calculated as 1407, 852, 879, 1282, and 1572 (ml H_2) (g of catalyst min)$^{-1}$ for Co amount, respectively. Additionally, the HGR of 1st, 2nd, 3rd, 4th, and 5th time metal loading were calculated as 252, 316, 492, 1263, and 2000 (ml H_2) (g of catalyst min)$^{-1}$ for 0.1 g p(VPA) microgel amount, respectively. As illustrated in Fig. 5b, parallel to the increased reloading numbers, the HGR per gram hydrogel is also increased. For the each new metal loading procedure, the microgels can loaded much more metal nanoparticles, and as the increase in the amounts of metal nanocatalyst increases, the increase hydrogen production rate is obtained for the same amount of microgel template. Together with the increase in magnetic responsiveness by increased amounts of Co nanoparticles maybe very useful for the control of catalytic behavior by an applied magnetic field from the outside of the system [18].

3.4. The effects of temperature on five times Co(II)-loaded and reduced p(VPA)–Co microgel for the hydrolysis reaction

Hydrolysis kinetics can be influenced by different factors such as catalyst performance and reaction temperature. Five times metal loaded 0.1 g p(VPA)–Co microgels (containing 1.29 mmol Co) were used to determine the effects of temperature on $NaBH_4$ and AB hydrolysis at 30, 50, and 70 °C under the same reaction conditions. As shown in Fig. 6, the temperature increase from 30 to 70 °C reduces the hydrolysis reaction time from 130 to 35 s for the $NaBH_4$ hydrolysis reaction and from 88 to 24 s for the AB hydrolysis reaction. From Table 4, The total TOF at 30, 50, and 70 °C were calculated as 3.69, 6.57, and 15.02 mol H_2 (mol metal min)$^{-1}$ for $NaBH_4$ hydrolysis reaction and 3.78, 6.79, and 15.59 mol H_2 (mol metal min)$^{-1}$ for AB hydrolysis reaction, respectively. The HGR at 30, 50, and 70 °C for $NaBH_4$ hydrolysis reaction were 1572, 2631, and 5681 (ml H_2) (g of metal min)$^{-1}$ and for AB were 1603, 2725, and 5855 (ml H_2) (g of metal min)$^{-1}$, respectively. According to the results, the increase in the temperature increases the HGR and the total TOF values for both $NaBH_4$ and AB hydrolysis reactions. From Table 4, the catalyst performance of 5 times metal loaded p(VPA)–Co microgels at 70 °C shows higher activity than bulk p(VPA)–Co and bulk p(AAm-co-VPA)–Co catalysts in the literature [27,28]. Moreover, the activation energies for hydrolysis of $NaBH_4$ and AB catalyzed by p(VPA)–Co microgels were calculated as 28.002 and 25.511 kJ mol^{-1}, respectively. These activation energies are approximately the same values for bulk p(VPA)–Co (23.01 kJ mol^{-1}) which provided the best catalytic performance in our previous studies with similar catalyst systems [18,27,28]. Yet, still the activation energies are lower than for Co on activated carbon supported catalyst that is 45.64 kJ mol^{-1} for $NaBH_4$ hydrolysis [32], and 56 kJ mol^{-1} for intrazeolite cobalt(0) nanoclusters [16], and 63 kJ mol^{-1} for PVP-stabilized Co(0) nanoclusters [33] for AB hydrolysis reaction reported in the literature.

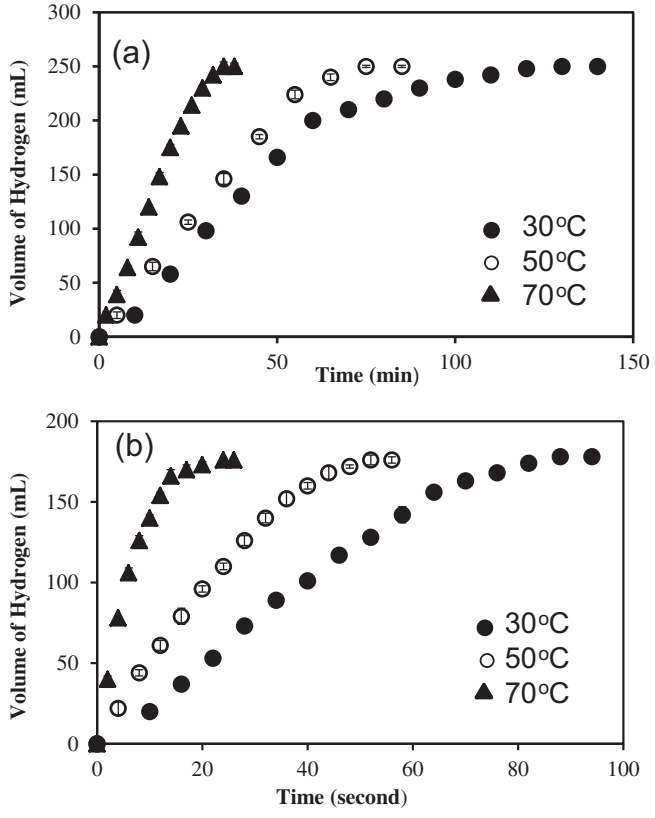

Fig. 6. The effect of temperature on (a) $NaBH_4$ and (b) AB hydrolysis reaction [5th time metal loading of 0.1 g p(VPA)–Co microgels (containing 1.29 mmol Co) at 30, 50, 70 °C.

3.5. The reusability of p(VPA)–Co microgel in the hydrolysis reaction

To examine the % conversion and the activity, p(VPA)–Co microgel was used repeatedly in hydrolysis of $NaBH_4$ reaction ten times in a row in one day. As demonstrated in Table 5, the conversion was 100% each time, and the catalytic activity was the same at the end of the 3rd use, and reduced to 90% at the end of the 10th use. The activity is calculated based on the hydrolysis of the reaction rate relative to the initial rate after each use. Our previous study revealed that the catalytic activity of bulk p(VPA)–Co is significantly reduced to 15 ± 8% after 5th use, whereas, p(VPA)–Co microgel has very good catalytic activity and performance.

3.6. The effect on the catalytic performance of p(VPA)–Co microgel in the hydrolysis reaction

To realize whether the porosity of p(VPA) matrix have any effect on hydrogen production rate from the hydrolysis of $NaBH_4$, the same amount of Co nanoparticle (0.232 mmol Co) containing 0.1 g p(VPA)–Co, and 0.077 g porous p(VPA)–Co composite microgels were used as catalyst systems in the hydrolysis of $NaBH_4$ under same reaction contains (50 mM 50 ml aqueous $NaBH_4$ solution containing 5 wt % NaOH, at 30 °C, 1000 rpm). As illustrated in Fig. 7, the porous material produce the same amounts of hydrogel (~246 ml) in 8 min whereas the nonporous p(VPA)–Co system produced about 12 min. Also, from the slope of the curves presented in Fig. 7, the hydrogen production rate of porous p(VPA)–Co is much faster than p(VPA)–Co, non porous one, and HGRs for porous p(VPA)–Co and p(VPA)–Co microgels were calculated as 2033 and 1407 (ml H_2) (g of Co min)$^{-1}$, respectively. Accordingly, the porosity in the microgel can generate high metal ion loading capacity, and fast hydrogen production rates. It very well known that increasing the surface area, and porosity of catalysts significantly enhances the catalytic activity. Surface areas measurements of p(VPA) and porous p(VPA) microgels were also evaluated by N_2

Table 5
The catalytic performances of p(VPA)–Co microgel catalyst system in terms of conversion and activity in ten consecutive uses for the hydrolysis of $NaBH_4$.

Run number	1	2	3	4	5	6	7	8	9	10
% Conversion	100	100	100	100	100	100	100	100	100	100
% Activity	100	100 ± 2	100 ± 1	99 ± 1	96 ± 3	96 ± 3	96 ± 2	96 ± 2	94 ± 1	90 ± 2

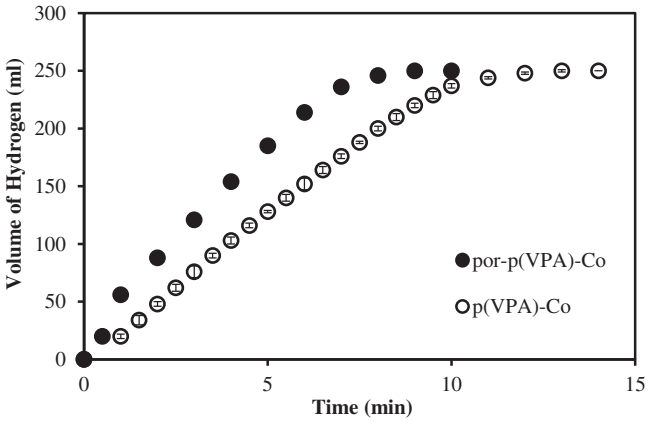

Fig. 7. The catalytic effects of 0.232 mmol p(VPA) and porous p(VPA)–Co composite micro particles 50 mM 50 ml aqueous $NaBH_4$ solution containing 5 wt % NaOH, at 30 °C, 1000 rpm.

adsorption/desorption isotherms. The values of the BET area was measured as 1.64, 3.26, and 8.12 $m^2\ g^{-1}$ for porous p(VPA), p(VPA)–Si, and p(VPA) in $P/P_0 = 0.05–0.3$ range. Additionally, it was found that p(VPA) microgels have pore sizes of 17.4 nm, whereas p(VPA)–Si and porous p(VPA) microgels have 25.1 and 60.2 nm pore sizes, respectively. The pore volumes of the microgels were measured as 0.04, 0.012, and 0.017 $cm^3\ g^{-1}$ for p(VPA), p(VPA)–Si, porous p(VPA), respectively. Therefore, the ability to generate pores in p(VPA) is also another advantage for fast hydrogen generation and also provide advantages for faster absorption of metal species, and applicable for other kinds of reactions.

As a result, we demonstrated here that p(VPA) microgels provided better catalytic performance in the hydrolysis of $NaBH_4$, and AB in many aspects. For example, upon comparison to macro p(VPA) hydrogels, p(VPA) microgel provided better properties such as higher surface area, pore structure, and faster hydrogen production rates and TOF values, and inherently magnetic behavior after multiple loading-reduction steps of Co(II) from aqueous medium. These kinds of materials can be used for controllable H_2 generation for various power sources.

4. Conclusion

P(VPA) and porous p(VPA) microgel were firstly synthesized and used as template to prepare Co, Ni, and Cu nanoparticles for generation of H_2. In this study, we report composite p(VPA) microgel that can be used for Co(II) loading several times and as porous structures with silica particles. The most important outcome of this research is that the prepared Co nanoparticles are inherently magnetic field responsive and can be used both for the hydrolysis of $NaBH_4$ and AB and as magnetic field responsive materials. The magnetic field responsive and tunable microgel based on p(VPA) has many potential applications and can also be used for other types of catalytic reactions. Moreover, (10.8 wt %) for $NaBH_4$ and (19.6 wt %) for AB.

Acknowledgments

This work is supported by the Scientific and Technological Research Council of Turkey. (110T649).

References

[1] J.K. Oha, D.I. Leea, J.M. Park, Prog. Polym. Sci. 34 (2009) 1261–1282.
[2] C. Chang, L. Zhang, Carbohydr. Polym. 84 (2011) 40–53.
[3] M. Malmsten, H. Bysell, P. Hansson, Curr. Opin. Colloid Interface Sci. 15 (2010) 435–444.
[4] W. Wu, J. Shen, P. Banerjee, S. Zhou, Biomaterials 31 (2010) 8371–8381.
[5] M.D. Moya-Ortegaa, C. Alvarez-Lorenzob, A. Concheirob, T. Loftsson, Int. J. Pharm. 428 (2012) 152–163.
[6] K. Hettiarachchi, A.P. Lee, J. Colloid Interface Sci. 344 (2010) 521–527.
[7] G. Zenkl, T. Mayr, I. Khmant, Macromol. Biosci. 8 (2008) 146–152.
[8] M. Karg, T. Hellweg, Curr. Opin. Colloid Interface Sci. 14 (2009) 438–450.
[9] M. Ballauff, Y. Lu, Polymer 48 (2007) 1815–1823.
[10] M.T. Gokmen, F.E.D. Prez, Prog. Polym. Sci. 37 (2012) 365–405.
[11] T. Jesionowski, A. Krysztafkiewicz, Colloid Surf. A 207 (2002) 49–58.
[12] N. Sahiner, C. Silan, S. Sagbas, P. Ilgin, S. Butun, H. Erdugan, R.S. Ayyala, Microporous Mesoporous Mater. 155 (2012) 124–130.
[13] S. Sagbas, N. Sahiner, Int. J. Hydrogen Energy 37 (2012) 18944–18951.
[14] S.S. Muir, X. Yao, Int. J. Hydrogen Energy 36 (2011) 5983–5997.
[15] Y. Wanga, K.S. Chen, J. Mishler, S.C. Cho, X.C. Adroher, Appl. Energy 88 (2011) 981–1007.
[16] B.H. Liu, Z.P. Li, J. Power Sources 187 (2009) 527–534.
[17] N. Sahiner, O. Ozay, E. Inger, N. Aktas, Appl. Catal. A 102 (2011) 201–206.
[18] N. Sahiner, O. Ozay, E. Inger, N. Aktas, J. Power Sources 196 (2011) 10105–10111.
[19] S. Butun, N. Sahiner, Polymer 52 (2011) 4834–4840.
[20] O. Ozay, N. Aktas, E. Inger, N. Sahiner, Int. J. Hydrogen Energy 36 (2011) 1998–2006.
[21] P. Schexnailder, G. Schmidt, Colloid Polym. Sci. 287 (2009) 1–11.
[22] O. Ozay, E. Inger, N. Aktas, N. Sahiner, Int. J. Hydrogen Energy 36 (2011) 8209–8216.
[23] Y. Chen, H. Kim, Fuel Process. Technol. 89 (2008) 966–972.
[24] N. Sahiner, O. Ozay, N. Aktas, E. Inger, J. He, Int. J. Hydrogen Energy 36 (2011) 15250–15258.
[25] Y.Y. Liu, X.Y. Liu, J.M. Yang, D.L. Lin, X. Chen, L.S. Zha, Colloid Surf. A 393 (2012) 105–110.
[26] J.C. Walter, A. Zurawski, D. Montgomery, M. Thornburg, S. Revankar, J. Power Sources 179 (2008) 335–339.
[27] S. Sagbas, N. Sahiner, Fuel. Process. Technol. 104 (2012) 31–36.
[28] N. Sahiner, S. Sagbas, Colloid Surf. A 418 (2013) 76–83.
[29] J.Z. Zhao, H. Ma, J. Chen, Int. J. Hydrogen Energy 32 (2007) 4711–4716.
[30] C.H. Liu, B.H. Chen, C.L. Hsueh, J.R. Ku, M.S. Jeng, F. Tsau, Int. J. Hydrogen Energy 34 (2009) 2153–2163.
[31] U.B. Demirci, F. Garin, Catal. Commun. 9 (2008) 1167–1172.
[32] W. Ye, H. Zhang, D. Xu, L. Ma, B. Yi, J. Power Sources 164 (2007) 544–548.
[33] Ö. Metin, S. Özkar, Energy Fuels 2 (2009) 3517–3526.